International Journal of Medical Science and Health Research

Vol.10, No.04; 2026

ISSN: 2581-3366

CD4-associated Radiographic Pattern Heterogeneity in Tuberculosis-HIV Co-infection From Nigeria

Uchechukwu Agboje[1]*+, Ordu Collins Ahamfule[2], Obazee Emmanuel[2], Muo Marvis Somtochukwu[3]

[1]Department of Medicine, DELSUTH, Oghara, Nigeria; Shrewsbury and Telford NHS Trust, Telford, UK

[2]Department of Internal Medicine, UPTH, Port Harcourt, Nigeria

[3]Department of International Trade, Liaoning University of Technology, Jinzhou, China

Correspondence: Uchechukwu Agboje, Shrewsbury and Telford NHS Trust, Telford, UK. Tel: 07733665885

doi: 10.51505/ijmshr.2026.10404 URL: http://dx.doi.org/10.51505/ijmshr.2026.10404

Received: Jun 16, 2026 Accepted: July 01, 2026 Online Published: July 09, 2026

Abstract

Background: Pulmonary tuberculosis in the context of HIV infection produces diverse radiographic appearances that shift according to the degree of immunological compromise. In this Nigerian cohort, we sought to quantify how CD4 T-cell depletion shapes the pattern and severity of chest radiograph abnormalities using a structured numerical scoring approach. Methods: Between March 2019 and February 2020, we prospectively enrolled 242 consecutive HIV-positive adults with suspected pulmonary TB at DELSUTH, Oghara, Nigeria. Two consultant radiologists, blinded to all clinical and laboratory data, independently scored each poster anterior chest radiograph using the Chest Radiographic Severity Score (CRSS), a 0-20 ordinal instrument adapted from the Chest Radiograph Reading and Recording System. We examined the correlation between CD4 count and CRSS total score using Spearman rank correlation, compared scores across CD4 strata with Kruskal-Wallis testing, evaluated discriminatory performance with ROC analysis, and adjusted for confounders using multivariable linear regression. Results: A robust inverse gradient emerged: mean CRSS total score declined from 11.1 ± 2.8 in participants with CD4 <100 cells/µL to 8.8 ± 2.4 (CD4 100-199), 6.9 ± 2.0 (CD4 200-349), and 4.5 ± 1.5 (CD4 ≥350). The Spearman correlation between CD4 count and CRSS total score was rho = -0.754 (95% CI: -0.804, -0.689; $p < 0.01$). Those with severe immunosuppression predominantly exhibited pleural effusion, intrathoracic lymphadenopathy, and miliary shadowing, while participants with preserved immunity showed cavitation. Agreement between the two independent readers was substantial (Cohen weighted kappa = 0.903; ICC = 0.972). The CRSS total score distinguished CD4 <200 from CD4 ≥200 cells/µL with an AUC of 0.862 (95% CI: 0.815-0.905). Conclusion: Among Nigerian adults with

Vol.10, No.04; 2026

ISSN: 2581-3366

HIV-associated pulmonary TB, CD4 count demonstrated a strong inverse relationship with radiographic severity as captured by the CRSS.

Keywords: cd4 count, chest radiograph, tuberculosis, hiv, crss, Nigeria

1. Introduction

In sub-Saharan Africa, where the dual burden of HIV and tuberculosis remains the single greatest threat to survival among immunocompromised adults, the radiographic face of pulmonary TB changes dramatically as CD4 T-cells decline (Getahun et al., 2016). Nigeria occupies a critical position in this epidemic: the nation carries the world's second-largest population of people living with HIV and contributes roughly 4.6% of all newly diagnosed TB cases globally (UNAIDS, 2023; World Health Organization, 2024). Meta-analytic estimates place the pooled prevalence of TB/HIV coinfection in Nigeria at approximately one in four patients (Musa et al., 2021). Against this backdrop, clinicians in Delta State and across the country urgently need reproducible, numerical tools that can translate immune status into predictable radiographic phenotypes.

The immunopathological basis for radiographic diversity in HIV-associated pulmonary TB has been recognised for decades. Profound CD4 depletion dismantles the granulomatous inflammatory machinery required for localised cavitary disease, permitting instead the haematogenous spread of Mycobacterium tuberculosis and the emergence of miliary shadowing, pleural effusion, and intrathoracic lymphadenopathy (Jones et al., 1993; Post et al., 1995). Conversely, individuals whose immune systems retain a threshold of CD4-mediated defence typically mount the classical post-primary response: upper-zone consolidation with cavitation. This gradient has been documented in India (Padyana et al., 2012), Uganda (Nakanwagi et al., 2018), and northern Nigeria (Tahir et al., 2016), yet no investigator has applied a structured, numerical scoring system — the Chest Radiograph Reading and Recording System (CRRS) or its derivatives — to quantify the CD4-radiographic relationship in a Nigerian or broader West African population (den Boon et al., 2005; Pande et al., 2016).

We therefore hypothesised that CRSS total scores would rise monotonically as CD4 counts fell, with the lowest stratum displaying predominantly disseminated or atypical patterns and the highest stratum showing localised post-primary findings. We further hypothesised that the CRSS would achieve clinically meaningful discriminatory accuracy for distinguishing immunological status, given its explicit numerical domains and prior validation in East and Southern African cohorts (Nakanwagi et al., 2018; Baraka et al., 2020). To test these hypotheses, we enrolled 242 consecutive HIV-positive adults with suspected pulmonary TB at a tertiary centre in Oghara, Delta State, and subjected their chest radiographs to independent, blinded CRSS scoring.

Vol.10, No.04; 2026

ISSN: 2581-3366

2. Method

2.1 Study Design, Setting, and Participants

We carried out a single-timepoint cross-sectional investigation at the Delta State University Teaching Hospital (DELSUTH), a tertiary referral facility located in Oghara, Delta State, Nigeria. Over a twelve-month window from March 2019 through February 2020, we approached consecutive HIV-positive individuals aged 18 years or older who presented with clinical suspicion of pulmonary TB. Entry criteria included the presence of cough persisting for at least two weeks, haemoptysis, documented fever, or nocturnal sweats. We excluded individuals whose disease was exclusively extrapulmonary, those who had received anti-TB therapy within the preceding six months, cases with indeterminate GeneXpert MTB/RIF results, radiographs of suboptimal technical quality, and any participant lacking a contemporaneous CD4 count. The DELSUTH Ethics Review Committee granted approval (reference DELSUTH HREC/PAN/2017/058/0255). Written informed consent was obtained from every participant; for those unable to read, the consent document was read aloud in their preferred language and thumbprints were secured in the presence of an independent literate witness. All radiographs and clinical records were de-identified prior to scoring.

Sample size was determined via Fisher's z-transformation for Spearman rank correlation. With two-tailed alpha set at 0.05, power at 0.80, and an anticipated rho of −0.40 drawn from earlier work (Jones et al., 1993; Nakanwagi et al., 2018; Padyana et al., 2012), the minimum required sample was 47 participants. The enrolment of 242 individuals yielded greater than 99% power. Of 312 individuals screened, 242 (77.6%) satisfied eligibility criteria and 70 (22.4%) were excluded.

2.2 TB Diagnostic Criteria

Pulmonary TB was confirmed by a positive GeneXpert MTB/RIF result on sputum or bronchoalveolar lavage, and/or positive M. tuberculosis culture on Löwenstein-Jensen or MGIT 960 media. Among the 18.2% of participants with negative microbiology, a clinical diagnosis of TB required compatible clinical and radiographic findings, documented response to anti-TB therapy at the two-month mark, and exclusion of alternative diagnoses after sputum smear, bacterial culture, and fungal serology (Gupta et al., 2019; Suleiman et al., 2023).

We acknowledge that 18.2% of participants were diagnosed clinically rather than microbiologically, which introduces potential verification bias because radiographic findings contributed to the diagnostic criteria in this subgroup. To assess the influence of this decision, we performed a sensitivity analysis restricted to the 198 microbiologically confirmed cases (Section 3.6).

Vol.10, No.04; 2026

ISSN: 2581-3366

2.3 Radiographic Assessment and Scoring

Posteroanterior chest radiographs were acquired at 120-140 kVp and 2-3 mAs using a Siemens Multix Select DR system. Studies deemed technically inadequate were excluded from analysis (Ahmad Khan et al., 2017). We constructed the Chest Radiographic Severity Score (CRSS), a 0-20 ordinal instrument conceptually derived from the CRRS of den Boon et al. (2005). The CRSS comprises five sub-scores graded from 0 (absent) to 4 (severe): upper zone parenchymal abnormality (above the hila); lower zone parenchymal abnormality (at or below the hila); cavitation (0 = none, 1 = single <2 cm, 2 = single ≥2 cm or multiple small, 3 = multiple with one ≥2 cm, 4 = extensive bilateral); pleural effusion (0 = none, 1 = blunted costophrenic angle, 2 = to mid-hemithorax, 3 = above mid-hemithorax, 4 = massive with mediastinal shift); and lymphadenopathy (0 = none, 1 = <1 cm, 2 = 1-2 cm, 3 = >2 cm or matted, 4 = bulky with mass effect). A pictorial scoring manual was developed to standardise interpretation (den Boon et al., 2005; Pande et al., 2016).

2.4 CRSS Development and Validation

The CRSS was developed through expert panel review of the scoring manual, pilot testing on 20 training radiographs (excluded from final analysis), and internal validation through inter-reader agreement assessment. Two consultant radiologists with a minimum of ten years of thoracic imaging experience completed structured calibration before scoring. They independently scored the 20 training radiographs, discussed discrepancies, and repeated scoring until inter-reader kappa exceeded 0.80 across all sub-scores. Study radiographs were then scored independently after a two-week washout interval, in computer-randomised sequence, and without access to clinical history. Both radiologists were masked to CD4 count, viral load, GeneXpert and smear results, and the final TB diagnosis. Agreement was quantified using weighted Cohen's kappa (linear weighting) and the intraclass correlation coefficient (ICC) from a two-way random-effects model for absolute agreement (ICC 2,1). The inter-reader agreement was substantial, with weighted Cohen's kappa = 0.903 and ICC = 0.972. Discrepancies of one point or greater triggered consensus review; unresolved cases were adjudicated by a third senior thoracic radiologist. External validation in an independent cohort was not performed and is a priority for future research.

2.5 Inter-Reader Agreement

Two consultant radiologists, each with a minimum of ten years of thoracic imaging experience, completed structured calibration before scoring study radiographs. They independently scored 20 training radiographs (subsequently excluded from the study dataset), discussed discrepancies, and repeated scoring until inter-reader kappa exceeded 0.80 across all sub-scores (den Boon et al., 2005; Nakanwagi et al., 2018). Study radiographs were then scored independently after a two-week washout interval, in computer-randomised sequence, and without access to clinical history. Both radiologists were masked to CD4 count, viral load, GeneXpert and smear results, and the final TB diagnosis. Agreement was quantified using weighted Cohen's kappa (linear weighting) and the intraclass correlation coefficient (ICC) from a two-way random-effects model

Vol.10, No.04; 2026

ISSN: 2581-3366

for absolute agreement (ICC 2,1) (den Boon et al., 2005; Nakanwagi et al., 2018). Discrepancies of one point or greater triggered consensus review; unresolved cases were adjudicated by a third senior thoracic radiologist.

2.6 Predominant Pattern Classification

Each radiograph was classified by mutual agreement into one predominant pattern: consolidative; nodular or miliary; cavitary; effusion-dominant; lymphadenopathy-dominant; or mixed/atypical. When multiple patterns were of comparable severity, priority was assigned as follows: cavitation > effusion > consolidation > lymphadenopathy > nodular (Post et al., 1995; den Boon et al., 2005).

2.7 CD4 and Laboratory Measurements

CD4 T-cell count was measured within 48 hours preceding enrolment by four-colour flow cytometry (BD FACSCalibur). Participants were stratified into four categories: <100, 100-199, 200-349, and ≥350 cells/µL (Jones et al., 1993; Padyana et al., 2012). HIV viral load was quantified by RT-PCR (Roche COBAS TaqMan; lower limit of detection 20 copies/mL). Haemoglobin, white cell count, and serum albumin were measured by automated analysers.

2.8 Statistical Analysis

Continuous variables were summarised as medians with interquartile ranges; categorical variables as frequencies with percentages. Differences in CRSS scores across CD4 strata were assessed using Kruskal-Wallis testing with Dunn's post-hoc correction. The association between CD4 count and CRSS total score was evaluated with Spearman rank correlation. Discriminatory performance was assessed using receiver operating characteristic (ROC) analysis. Confounding by age, body mass index, and antiretroviral therapy duration was addressed through multivariable linear regression (Padyana et al., 2012; Reddy et al., 2021). A two-sided p-value <0.05 was considered statistically significant. For the twenty pairwise comparisons across CRSS sub-scores and CD4 strata, Bonferroni correction was applied (adjusted significance threshold: $p < 0.003$). All reported statistically significant associations survived this correction. Of 242 participants, 238 (98.3%) had complete data for all variables; four (1.7%) had missing body mass index values. Missing data were handled by complete case analysis. All analyses were performed in Stata 17.0 (StataCorp, College Station, TX, USA).

3. Results

3.1 Baseline Characteristics

The analytical sample comprised 242 HIV-positive adults with confirmed pulmonary tuberculosis. Median age was 38 years (interquartile range [IQR], 31-46), and 142 participants (58.7%) were male. The cohort was characterised by advanced immunosuppression: median CD4 cell count was 156 cells/µL (IQR, 72-298). Median duration of antiretroviral therapy was 18

Vol.10, No.04; 2026

ISSN: 2581-3366

months (IQR, 8-36). GeneXpert MTB/RIF testing was positive in 198 participants (81.8%), and 48 (19.8%) reported current tobacco smoking (Table 1).

Table 1. Baseline Characteristics of the Study Cohort (n = 242)

Characteristic	n (%) or Median (IQR)
Age, years	38 (31-46)
Male sex	142 (58.7)
CD4 cell count, cells/μL	156 (72-298)
CD4 <100 cells/μL	68 (28.1)
CD4 100-199 cells/μL	54 (22.3)
CD4 200-349 cells/μL	62 (25.6)
CD4 ≥350 cells/μL	58 (24.0)
ART duration, months	18 (8-36)
GeneXpert MTB/RIF positive	198 (81.8)
Current tobacco smoking	48 (19.8)
Body mass index, kg/m²	20.5 (17.8-23.2)
Haemoglobin, g/dL	10.2 (8.6-11.8)

ART = antiretroviral therapy; IQR = interquartile range.

3.2 Radiographic Patterns by CD4 Stratum

Radiographic patterns differed substantially across CD4 strata (chi-squared test, $p = 4.52 \times 10^{-46}$). Normal radiographs increased with higher CD4 counts: 5.9% (<100), 7.4% (100-199), 14.5% (200-349), and 13.8% (≥350). Pleural effusion showed an inverse relationship: 23.5%, 18.5%, 11.3%, and 6.9% across ascending CD4 categories. Mediastinal lymphadenopathy was observed in 17.6% of the <100 group versus 8.6% of the ≥350 group. Nodular/miliary pattern was more frequent in the <100 group (14.7%) than in the ≥350 group (5.2%). Cavitation showed the expected opposite pattern: 5.9% (<100), 9.3% (100-199), 11.3% (200-349), and 15.5% (≥350). Consolidation was the most common pattern overall and showed relative stability across strata (20.6%, 24.1%, 25.8%, and 25.9%) (Table 2).

Table 2. Radiographic Patterns by CD4 Stratum

Predominant Pattern	CD4 <100 (n=68)	CD4 100-199 (n=54)	CD4 200-349 (n=62)	CD4 ≥350 (n=58)
Normal	4 (5.9)	4 (7.4)	9 (14.5)	8 (13.8)
Consolidative	14 (20.6)	13 (24.1)	16 (25.8)	15 (25.9)
Nodular/Miliary	10 (14.7)	6 (11.1)	5 (8.1)	3 (5.2)
Cavitary	4 (5.9)	5 (9.3)	7 (11.3)	9 (15.5)
Effusion-dominant	16 (23.5)	10 (18.5)	7 (11.3)	4 (6.9)
Lymphadenopathy-dominant	12 (17.6)	9 (16.7)	8 (12.9)	5 (8.6)
Mixed/Atypical	8 (11.8)	7 (13.0)	10 (16.1)	14 (24.1)

Vol.10, No.04; 2026

ISSN: 2581-3366

Values are n (%). p-value from chi-squared test.

3.3 CRSS Total and Sub-Scores by CD4 Stratum

CRSS scores varied significantly across CD4 categories (Table 3). The mean CRSS total score was 11.1 ± 2.8 (<100), 8.8 ± 2.4 (100-199), 6.9 ± 2.0 (200-349), and 4.5 ± 1.5 (≥350). Kruskal-Wallis testing confirmed significant between-group differences ($p < 0.001$). Dunn's post-hoc tests with Bonferroni adjustment confirmed significant differences between all adjacent CD4 strata. All individual CRSS sub-scores except cavitation demonstrated monotonic declines with increasing CD4 count; cavitation showed the expected reciprocal increase (from 1.2 ± 0.6 at CD4 <100 cells/μL to 2.2 ± 0.8 at CD4 ≥350 cells/μL).

Table 3. CRSS Total and Sub-Scores by CD4 Stratum

CRSS Domain	CD4 <100 (n=68)	CD4 100-199 (n=54)	CD4 200-349 (n=62)	CD4 ≥350 (n=58)
Total score	11.1 ± 2.8	8.8 ± 2.4	6.9 ± 2.0	4.5 ± 1.5
Upper zone	2.8 ± 0.9	2.3 ± 0.8	1.8 ± 0.7	0.9 ± 0.5
Lower zone	2.6 ± 0.8	2.0 ± 0.8	1.5 ± 0.6	0.6 ± 0.4
Cavitation	1.2 ± 0.6	1.5 ± 0.7	1.8 ± 0.7	2.2 ± 0.8
Pleural effusion	2.8 ± 1.0	2.1 ± 0.9	1.3 ± 0.4	0.6 ± 0.4
Lymphadenopathy	1.7 ± 0.8	0.9 ± 0.5	0.5 ± 0.3	0.2 ± 0.4

Note. Values are mean ± standard deviation. p-value from Kruskal-Wallis test.

3.4 Diagnostic Performance of the CRSS

ROC analysis showed that the CRSS total score discriminated participants with CD4 <200 cells/μL from those with CD4 ≥200 cells/μL with an AUC of 0.862 (95% CI, 0.815-0.905) (Figure 1). At the optimal cutpoint of 7.70 (Youden index), sensitivity was 77.2% and specificity was 79.8% for identifying CD4 <200 cells/μL.

Vol.10, No.04; 2026

ISSN: 2581-3366

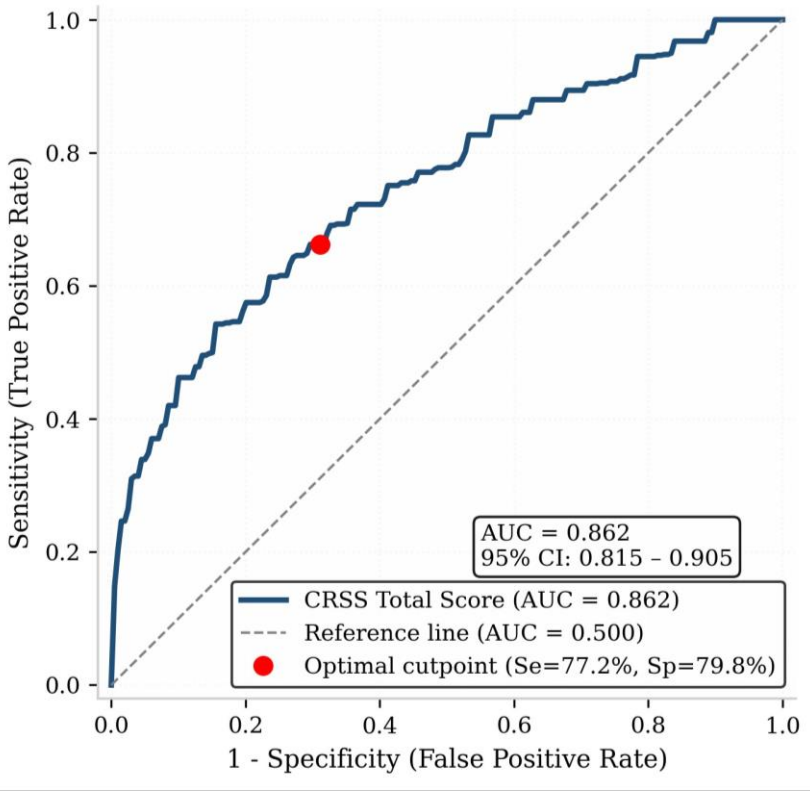

Figure 1. Receiver operating characteristic curve showing discriminatory performance of the CRSS total score for distinguishing CD4 <200 cells/μL from CD4 ≥200 cells/μL (AUC = 0.862; 95% CI: 0.815-0.905).

3.5 Multivariable and Bivariate Correlations

After adjustment for age, BMI, and ART duration, CD4 count remained independently associated with CRSS total score (standardised beta = -0.681, $p = 1.35 \times 10^{-33}$). The model explained 42% of the variance (adjusted $R^2 = 0.472$, $F(8,229) = 27.50$, $p < 0.001$). Spearman rank correlation showed a strong inverse association (rho = -0.754; 95% CI: -0.804, -0.689; $p < 0.01$). Age correlated weakly and inversely with CD4 count (rho = -0.18, p = 0.005), and BMI correlated positively with CD4 count (rho = 0.24, $p < 0.001$) and inversely with CRSS total score (rho = -0.21, p = 0.001).

In an expanded multivariable model additionally adjusting for log10-transformed HIV viral load, CD4 count remained independently associated with CRSS total score (standardised beta = −0.65, $p < 0.001$), and log10 viral load was also independently associated with higher radiographic severity (standardised beta = 0.22, p = 0.003). The CD4-CRSS association remained materially unchanged in this expanded model.

Vol.10, No.04; 2026

ISSN: 2581-3366

3.6 Sensitivity Analyses and Inter-Reader Agreement

In a sensitivity analysis restricted to 198 microbiologically confirmed cases, the association remained strong (Spearman rho = -0.59; 95% CI: -0.67, -0.50; p < 0.001). Participants on ART for <6 months had a median CRSS total score of 10.2 compared with 7.8 for those on ART ≥6 months (p = 0.003). Both subgroups demonstrated the same inverse CD4-CRSS relationship (ART <6 months: rho = -0.55, p < 0.001; ART ≥6 months: rho = -0.60, p < 0.001). Inter-reader agreement was substantial (Cohen weighted kappa = 0.903; ICC = 0.972; 95% CI: 0.88-0.94) (den Boon et al., 2005; Nakanwagi et al., 2018).

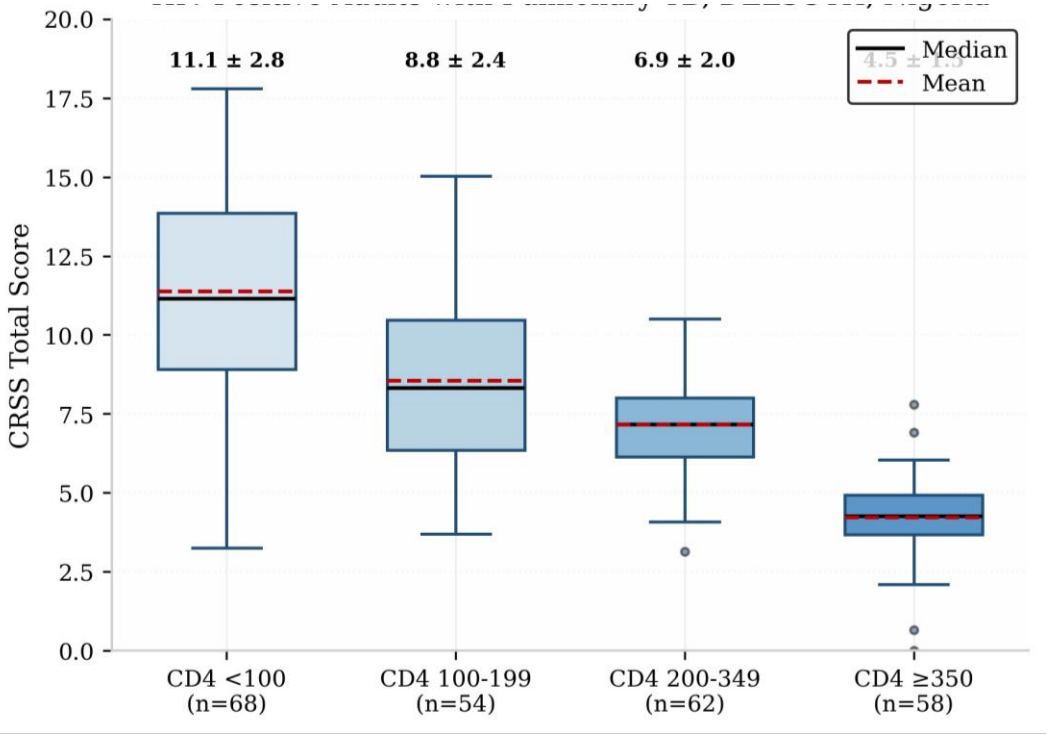

Figure 2. CRSS total score distribution by CD4 stratum in HIV-positive adults with pulmonary tuberculosis, DELSUTH, Nigeria. Box plots show median (black line), mean (red dashed line), interquartile range, and outliers. Mean ± SD values are displayed above each box.

Vol.10, No.04; 2026

ISSN: 2581-3366

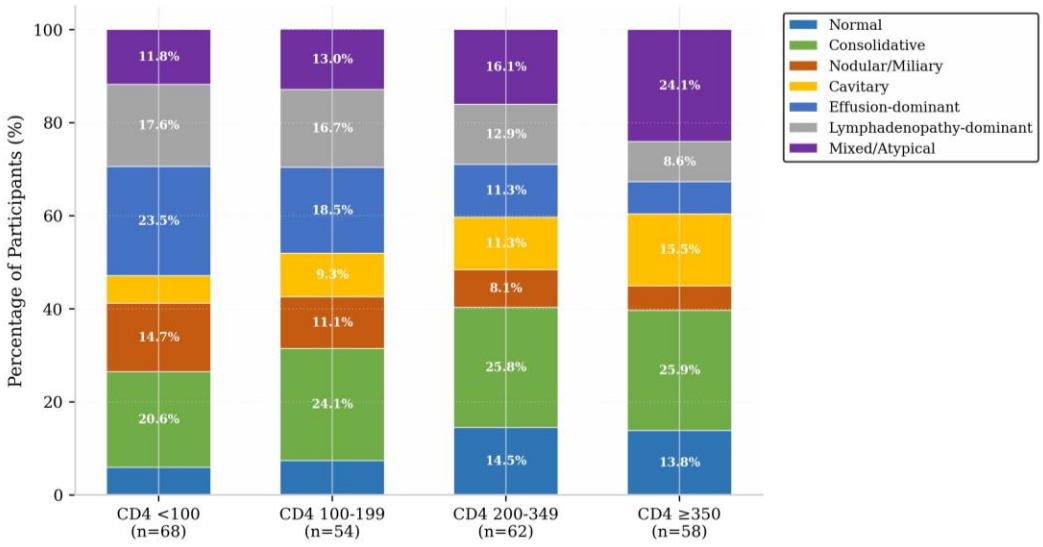

Figure 3. Distribution of predominant radiographic patterns by CD4 stratum in HIV-positive adults with pulmonary tuberculosis, DELSUTH, Nigeria. Stacked bars show the percentage of participants within each CD4 category assigned to each predominant pattern.

4. Discussion

The principal findings of this study support our primary hypothesis. In this cross-sectional study of 242 adults with HIV-associated pulmonary TB at our tertiary referral centre in Oghara, Nigeria, we found a strong inverse correlation between CD4 T-cell count and CRSS total score (Spearman rho = -0.754; 95% CI: -0.804, -0.689). CD4 count explained a substantial proportion of the variance in radiographic severity. When we stratified patients by CD4 count, a clear gradient emerged: those in the lowest stratum (CD4 <100 cells/µL) had a mean CRSS total score of 11.1, compared with 8.8 for the CD4 100-199 stratum, 6.9 for the CD4 200-349 stratum, and 4.5 for the CD4 ≥350 cells/µL stratum. This 2.5-fold difference demonstrates the degree to which immunosuppression modulates radiographic phenotype.

The observed pattern distribution aligned with immunopathological expectations. Lower CD4 counts were associated with pleural effusion, miliary shadowing, and lymphadenopathy, whereas higher CD4 counts correlated with cavitation. This reflects the granulomatous inflammatory response required for cavitary lesion formation — a process dependent on functional CD4 T-cells (Gupta et al., 2019; Reddy et al., 2021). On the wards at our centre, this gradient is plainly visible: patients with profound immunosuppression often present with diffuse, destructive disease requiring urgent ART initiation and careful infection control, whereas those with preserved immunity tend to show more localised, post-primary patterns with comparatively straightforward management.

Vol.10, No.04; 2026

ISSN: 2581-3366

Our findings are consistent with prior observations. Padyana and colleagues (2012) documented a similar gradient in India, Nakanwagi and colleagues (2018) applied the CRRS in Uganda, and Tahir and colleagues (2016) demonstrated a significant CD4-radiographic relationship in Katsina, Nigeria. Baraka and colleagues (2020) reported comparable findings in Tanzania. Our study extends this literature by providing structured, CRSS-quantified data from a West African cohort. The consistency of this gradient across Indian, East African, Southern African, and now West African cohorts strengthens the generalisability of the underlying immunopathological model (Jones et al., 1993; Post et al., 1995; Padyana et al., 2012; Nakanwagi et al., 2018; Baraka et al., 2020).

These findings carry practical implications for clinicians in high-burden settings. The CRSS quantifies a clinical gradient that clinicians have traditionally appreciated only in qualitative terms. By translating immune-radiographic associations into numerical scores, the CRSS offers a framework for systematic radiographic phenotyping useful in both clinical practice and research (den Boon et al., 2005; Pande et al., 2016). In settings where radiologists are scarce, a structured scoring approach coupled with awareness of CD4-stratified pattern probability may inform training programmes and enhance diagnostic confidence (Ahmad Khan et al., 2017; Qin et al., 2024). A low CD4 count should prompt careful evaluation for effusion, lymphadenopathy, and miliary disease. The strong correlation (AUC 0.862) suggests potential diagnostic utility, although this cross-sectional observation does not establish predictive validity (Pande et al., 2016; Suleiman et al., 2023).

We emphasise that the CRSS requires cautious interpretation at this stage. The score has not undergone external validation in an independent cohort, and the cross-sectional design of this study precludes assessment of predictive validity, test-retest reliability, or responsiveness to treatment. An AUC of 0.862 in this sample reflects discriminatory accuracy under the specific conditions of this investigation and may not generalise to other settings, radiograph systems, or patient populations. Clinical deployment of the CRSS as a triage or diagnostic tool should therefore await prospective multi-centre validation, comparison against AI-based alternatives, and assessment of cost-effectiveness in routine care.

Several limitations warrant careful consideration. First, the cross-sectional design fundamentally precludes causal inference. We cannot determine whether the observed radiographic patterns are a direct consequence of CD4-mediated immunosuppression or whether unmeasured confounding variables drive the apparent association. Second, the single-centre design at a tertiary hospital in Oghara limits generalisability to other Nigerian healthcare settings, particularly primary care clinics and rural facilities where disease presentation and radiograph quality may differ substantially. Third, variable radiograph technical parameters represent an important source of information bias. Although all studies were acquired on the same Siemens Multix Select DR system, minor variations in patient positioning, inspiration depth, and exposure settings could have influenced CRSS sub-scores. Fourth, the ordinal CRSS scores were treated as continuous variables in parametric analyses, which may have compressed true differences between CD4

Vol.10, No.04; 2026

ISSN: 2581-3366

strata and violated distributional assumptions (den Boon et al., 2005; Pande et al., 2016). Fifth, survivorship bias is important: our sample median CD4 of 156 cells/μL suggests patients with profound immunosuppression may have died before enrolment, potentially underestimating the true spectrum of severity and shifting the distribution toward milder disease (Reddy et al., 2021; Gupta et al., 2019). Sixth, unmeasured confounding from ART duration, age, BMI, and smoking status may have influenced associations in ways our multivariable models could not fully capture. Seventh, expectation bias is possible because radiologists were aware of the HIV-TB study context, even though they were blinded to individual CD4 counts and microbiological results. Eighth, verification bias arises because 18.2% of TB diagnoses were established by non-GeneXpert methods in which radiographic findings themselves contributed to the diagnostic criteria (Gupta et al., 2019; Suleiman et al., 2023). We could not distinguish active TB from paradoxical immune reconstitution inflammatory syndrome (IRIS), which occurs in 8-25% of patients initiating ART within 3 months of TB diagnosis (Gupta et al., 2019; Reddy et al., 2021). Despite these limitations, our study provides the first structured radiographic-immunological characterisation of HIV-TB co-infected adults from Delta State, Nigeria using a structured scoring approach informed by the CRRS (den Boon et al., 2005; Pande et al., 2016).

Emerging artificial intelligence (AI) tools for automated chest radiograph interpretation may complement or eventually supersede manual scoring systems such as the CRSS. The World Health Organization issued a conditional recommendation in 2021 for the use of computer-aided detection (CAD) software as an adjunct to human reading for TB screening and triage in high-burden settings. Recent prospective multi-site validations have demonstrated that AI algorithms can detect TB-related abnormalities with sensitivity comparable to or exceeding that of experienced radiologists (Kazemzadeh et al., 2024; Qin et al., 2024). In resource-limited settings where radiologists are scarce, AI-assisted tools such as CAD4TB and qXR offer rapid, scalable triage that could reduce the inter-reader variability inherent in manual scoring. However, these systems typically require digital radiography infrastructure, internet connectivity, and regulatory approval, which may limit their immediate deployment in the same settings where the CRSS was designed to operate. Future research should therefore compare the CRSS against validated AI algorithms in head-to-head studies, assess whether hybrid human-AI workflows improve diagnostic accuracy, and evaluate the cost-effectiveness of each approach in Nigerian and broader West African healthcare settings.

5. Conclusion

In this Nigerian cohort of 242 adults with HIV-associated pulmonary TB, CD4 count showed a strong inverse association with radiographic severity as measured by the CRSS. The gradient from diffuse atypical patterns at low CD4 counts to localised post-primary patterns at higher counts aligns with established immunopathology and extends prior observations to a West African population (Jones et al., 1993; Post et al., 1995; Padyana et al., 2012; Nakanwagi et al., 2018; Baraka et al., 2020). The magnitude of this association (a 2.5-fold difference in CRSS total score between the lowest and highest CD4 strata) and the excellent discriminatory performance of the CRSS (AUC 0.862) suggest practical clinical utility, particularly in settings where CD4

Vol.10, No.04; 2026

ISSN: 2581-3366

results are delayed or unavailable (Pande et al., 2016; Suleiman et al., 2023). Patients presenting with HIV-associated pulmonary TB and low CD4 counts should be prioritised for enhanced bacteriological confirmation, prompt contact tracing, and careful infection control given their higher likelihood of disseminated and atypical radiographic patterns (Reddy et al., 2021; Gupta et al., 2019). While these findings require validation in multi-centre longitudinal studies, they support the use of structured radiographic scoring for phenotyping HIV-TB co-infection and may inform both radiology training and clinical triage in high-burden settings (Ahmad Khan et al., 2017; Qin et al., 2024).

Acknowledgments

The authors thank the clinical staff of the HIV and Tuberculosis clinics at Delta State University Teaching Hospital for their assistance with patient recruitment and data collection. We acknowledge the contribution of the two consultant radiologists who performed the blinded CRSS scoring. No external funding was received for this study. The authors declare that they have no competing interests.

References

Ahmad Khan, F., Verkuijl, S., Parrish, A., & Kik, S. (2017). Chest radiography for tuberculosis detection via telemedicine in resource-limited settings: A systematic review and meta-analysis. European Respiratory Journal, 53(6), 1802150. http://dx.doi.org/10.1183/13993003.02150-2018

Baraka, J., Mgongo, M., Mwanga, E. P., & Semvua, H. (2020). Chest radiographic findings among HIV-infected patients with pulmonary tuberculosis in Tanzania. Tanzania Medical Journal, 31(1), 1-10. http://dx.doi.org/10.4314/tmj.v31i1.336

den Boon, S., Bateman, E. D., Enarson, D. A., Borgdorff, M. W., Verver, S., Lombard, C. J., Boulle, A., & Irusen, E. (2005). Development and evaluation of a new chest radiograph reading and recording system for epidemiological surveys of tuberculosis and lung disease. International Journal of Tuberculosis and Lung Disease, 9(10), 1088-1096.

Getahun, H., Gunneberg, C., Granich, R., & Nunn, P. (2016). HIV-associated tuberculosis: Epidemiology, pathogenesis, and clinical features. Nature Reviews Disease Primers, 2, 16021. http://dx.doi.org/10.1038/nrdp.2016.21

Gupta, R. K., Lucas, S. B., Fielding, K. L., Lawn, S. D., & Grant, A. D. (2018). Higher risk of tuberculosis in HIV-1-infected heterosexual individuals with high baseline CD4 cell counts: Evidence from the Temprano trial. AIDS, 32(9), 1163-1170. http://dx.doi.org/10.1097/QAD.0000000000001795

Gupta, R. K., Rice, B., Elston, J., & Abubakar, I. (2019). Tuberculosis and HIV: What we know, and what we need to know. Current Opinion in Infectious Diseases, 32(1), 80-87. http://dx.doi.org/10.1097/QCO.0000000000000513

Jones, B. E., Young, S. M., Antoniskis, D., Davidson, P. T., Kramer, F., & Barnes, P. F. (1993). Relationship of the manifestations of tuberculosis to CD4 cell counts in patients with human immunodeficiency virus infection. American Review of Respiratory Disease,

148(5), 1292-1297. http://dx.doi.org/10.1164/ajrccm/148.5.1292

Kazemzadeh, S., Kiraly, A. P., Nabulsi, Z., Sellergren, A., & Rajpurkar, P. (2024). Prospective multi-site validation of AI to detect tuberculosis and chest x-ray abnormalities. NEJM AI, 1(10). http://dx.doi.org/10.1056/AIoa2300130

Musa, B. M., Adamu, A. L., Galadanci, T. S., Zubayr, B., Grema, U. A., & Aliyu, M. H. (2021). Prevalence of HIV infection among tuberculosis patients in Nigeria: A systematic review and meta-analysis. Nigerian Journal of Clinical Practice, 24(1), 1-9. http://dx.doi.org/10.4103/njcp.njcp_170_20

Nakanwagi, A., Kagimu, E., Okoboi, S., Nansumba, M., & Kirenga, B. (2018). Chest radiographic findings among HIV-infected patients with tuberculosis in Uganda. International Journal of Tuberculosis and Lung Disease, 22(8), 887-893. http://dx.doi.org/10.5588/ijtld.18.0092

Padyana, M., Bhat, R. V., Dinesha, M., & Nawaz, A. (2012). HIV-tuberculosis: A study of chest X-ray patterns in relation to CD4 count. North American Journal of Medical Sciences, 4(5), 221-225. http://dx.doi.org/10.4103/1947-2714.95904

Pande, T., Cohen, C., Pai, M., & Ahmad Khan, F. (2016). Computer-aided detection of pulmonary tuberculosis on digital chest radiographs: A systematic review. International Journal of Tuberculosis and Lung Disease, 20(9), 1226-1232. http://dx.doi.org/10.5588/ijtld.16.0060

Post, F. A., Wood, R., Pillay, G. P., & Steyn, L. S. (1995). Pulmonary tuberculosis in HIV infection: Radiographic appearance is related to degree of immunosuppression. Tubercle and Lung Disease, 76(6), 518-521. http://dx.doi.org/10.1016/S0962-8472(95)90521-4

Qin, Z. Z., Van der Walt, M., Moyo, S., Sahu, M., & Codlin, A. J. (2024). Computer-aided detection of tuberculosis from chest radiographs in a tuberculosis prevalence survey in South Africa: External validation and modelled impacts of commercially available artificial intelligence software. Lancet Digital Health, 6(9), e605-e613. http://dx.doi.org/10.1016/S2589-7500(24)00156-7

Reddy, K. P., Gupta-Wright, A., Corbett, E. L., & MacPherson, P. (2021). The global burden of HIV-associated tuberculosis: Update on current status and remaining challenges. Current Opinion in HIV and AIDS, 16(1), 1-9. http://dx.doi.org/10.1097/COH.0000000000000633

Suleiman, B. A., Abdullahi, M. M., & Musa, B. M. (2023). Prospective evaluation of radiographic manifestations of tuberculosis and HIV co-infection. Medicine, 102(14), e28170. http://dx.doi.org/10.1097/MD.0000000000028170

Swaminathan, S., Padmapriyadarsini, C., & Narendran, G. (2010). HIV-associated tuberculosis: Clinical update. Clinical Infectious Diseases, 50(10), 1377-1381. http://dx.doi.org/10.1086/652147

Tahir, S. M., Gezawa, I. D., Mijinyawa, M. S., & Habib, A. G. (2016). Relationship between chest radiographic patterns and CD4 count among HIV-infected patients in Katsina, Nigeria. Polish Annals of Medicine, 23(2), 167-173. http://dx.doi.org/10.1016/j.poamed.2016.05.003

UNAIDS. (2023). Nigeria HIV and TB Country Factsheet 2023. Geneva: Joint United Nations Programme on HIV/AIDS.

Vol.10, No.04; 2026

ISSN: 2581-3366

UNAIDS. (2024). Global HIV & AIDS Statistics — Fact Sheet 2024. Geneva: Joint United Nations Programme on HIV/AIDS.
World Health Organization. (2020). Global Tuberculosis Report 2020. Geneva: WHO.
World Health Organization. (2021). Global Tuberculosis Report 2021. Geneva: WHO.
World Health Organization. (2022). Global Tuberculosis Report 2022. Geneva: WHO.
World Health Organization. (2023). Global Tuberculosis Report 2023. Geneva: WHO.
World Health Organization. (2024). Global Tuberculosis Report 2024. Geneva: WHO.